Dalton Transactions

ROYAL SOCIETY OF CHEMISTRY

PAPER

View Article Online
View Journal | View Issue

Cite this: *Dalton Trans.*, 2025, **54**, 5458

A mononuclear zinc(II) complex and a tetranuclear copper(II) azametallacoronate with (*E*)-2-((2-(quinazolin-4-yl)hydrazono)methyl) phenol: structure and biological activity†

Chrisoula Kakoulidou,[a] Antonios G. Hatzidimitriou,[a] Konstantina C. Fylaktakidou *[b] and George Psomas *[a]

A quinazoline derivative containing a properly situated *o*-phenol ring, namely (*E*)-2-((2-(quinazolin-4-yl) hydrazono)methyl)phenol (**H_2L**), was synthesized in order to investigate the ability of this novel ligand for metal complexation. The interaction of deprotonated HL^- with Zn(II) resulted in the mononuclear complex $[Zn(HL)_2]\cdot 1.5CH_3OH\cdot H_2O$ (complex **1**). When doubly deprotonated ligand L^{-2} reacted with Cu(II), the tetranuclear complex $[Cu_4(L)_4(DMF)_4]\cdot 8H_2O$ (complex **2**) was isolated, which can be described as an azametallacoronate compound. All three compounds (**H_2L** and complexes **1** and **2**) were characterized by spectroscopic techniques and single-crystal X-ray crystallography. The biological profile of the compounds was evaluated in regard to their affinity for calf-thymus DNA, the ability to cleave supercoiled circular pBR322 plasmid DNA in the absence or presence of irradiation of various wavelengths (UVA, UVB and visible light), their binding with bovine serum albumin and their capacity to scavenge 1,1-diphenyl-picrylhydrazyl and 2,2′-azinobis-(3-ethylbenzothiazoline-6-sulfonic acid) radicals and to reduce H_2O_2. The compounds can bind tightly to calf-thymus DNA *via* intercalation, and do not induce notable cleavage of plasmid DNA. They can bind tightly and reversibly to the albumin and have shown moderate antioxidant activity.

Received 22nd December 2024,
Accepted 26th February 2025

DOI: 10.1039/d4dt03518f

rsc.li/dalton

1 Introduction

Zinc and copper are among the most abundant trace elements (second and third, respectively) in the human body.[1] They both have a crucial role in physiology (copper is involved in the development of connective tissues and bones,[1,2] while zinc is very important in maintaining membrane barrier structure and function[3]) and participate in the active center of many enzymes.[1] They co-exist in the active center of Cu–Zn superoxide dismutase (SOD), an enzyme that catalyzes the dismutation of superoxide radicals into the less harmful O_2 and H_2O_2, thus contributing to controlling oxidative damage in biological species.[1–3] The application of 'Baby Zinc' and ZnO to treat diarrhea in Asian and African countries and skin injuries and infections, respectively, is well-known.[3,4] Concerning copper, its use as a material in knobs and contact surfaces in hospitals results from its bacteriostatic activity.[5] In addition, in medicine, the copper(II)-indomethacin complex, called CuAlgesal®, is used for the treatment of arthritis and a mixture of copper(II)/N,N′-donor complexes, called Casiopeinas®, is in clinical trials being tested for its anticancer activity.[6,7] A series of Zn(II)[8–12] and Cu(II)[13–16] complexes have been reported in the literature regarding promising *in vitro* biological activities.

Metallacrowns (MCs) constitute a class of polynuclear complexes, having a cyclic structure analogous to crown ethers with the repeating pattern [–O–N–M–] in which the methylene carbons are replaced by transition metal ions and nitrogen atoms.[17–21] However, a limited class of MCs are the azametallacrowns (azaMCs) which bear the repeating unit [–N–N–M–] by replacing the O atom with a N atom.[22–27] In all cases, the formation of such compounds can be designed by involving diverse (mainly) trivalent metal ions such as Fe(III), Cr(III), Mn(III), Co(III), and Er(III)[23,24,26–34] or divalent metal ions such as Cu(II),[22] and by choosing appropriate polydentate organic ligands such as derivatives of pyrazole, triazole, hydrazide.[22–24,26,31,32] Metallacoronates (MCor) can be considered a special form of metallacrowns bearing the repeating

[a]*Department of General and Inorganic Chemistry, Faculty of Chemistry, Aristotle University of Thessaloniki, GR-54124 Thessaloniki, Greece. E-mail: gepsomas@chem.auth.gr*
[b]*Laboratory of Organic Chemistry, Faculty of Chemistry, Aristotle University of Thessaloniki, GR-54124 Thessaloniki, Greece. E-mail: kfylakta@chem.auth.gr*

†Electronic supplementary information (ESI) available. CCDC 2401516–2401518. For ESI and crystallographic data in CIF or other electronic format see DOI: https://doi.org/10.1039/d4dt03518f

motif [–O–C–O–M–],[35–38] while just one report concerning analogous azametallacoronates (azaMCor) with a structural motif [–N–C–N–M–] was found in the literature.[39]

As a continuation of our previous project regarding the synthesis and characterization of derivatives (*E*)-4-(2-((pyridin-2-yl) methylene)hydrazinyl)quinazoline (**L1**, Fig. 1) and its metal complexes,[40–43] we have designed, synthesized and characterized a phenol analogue of **L1**, namely (*E*)-2-((2-(quinazolin-4-yl) hydrazono)methyl)phenol (**H_2L**, Fig. 1) as a novel ligand by replacing the pyridine ring with a phenol ring. Besides the initial structural features of **L1** (nitrogen atoms providing multiple coordination sites and rigidity enabling DNA-intercalation),[40–43] the insertion of the phenol group is designed to provide the possibility of single and double deprotonation of the quinazoline derivative upon reactions with metal ions. The **H_2L** individual has been used as an intermediate for the synthesis of thiazolidinone and azetidinone heterocyclic attachments on the quinazoline scaffold taking advantage of the imine part of the hydrazone moiety, without, however, the participation of the phenol ring itself.[44,45] On the contrary, the phenol part of 2-Ph-**H_2L** derivatives have participated in reaction with $Zn(OAc)_2$ to form complexes that were found to have enhanced fluorescent quantum yields compared to their respective ligands due to increased rigidity of the system upon the complexation.[46] Finally, another 2-substituted quinazoline derivative, the 2,4-[bis-(2-hydroxy-3-methoxybenzylidene)]-dihydrazinoquinazoline was found to preferably emit fluorescence when interacted with Zn(II).[47]

Therefore, the reaction of **H_2L**, used as a novel ligand, with Zn(II) resulted in the mononuclear complex $[Zn(HL)_2]\cdot 1.5CH_3OH\cdot H_2O$ (complex **1**), while the reaction with Cu(II) yielded the tetranuclear complex $[Cu_4(L)_4(DMF)_4]\cdot 8H_2O$ (complex **2**) which can be described as an azametallacoronate [16-azaMCor-4] complex. The characterization of all three compounds was achieved by spectroscopic techniques (IR, UV-vis, ^{1}H NMR) and single-crystal X-ray crystallography.

The three compounds (**H_2L**, and novel complexes **1** and **2**) were further evaluated *in vitro* for their: (i) interaction with calf-thymus (CT) DNA studied by UV-vis spectroscopy, viscosity measurements, and *via* competitive studies with ethidium bromide (EB) by fluorescence emission spectroscopy, (ii) ability to cleave supercoiled circular pBR322 plasmid DNA (pDNA) in the absence or presence of irradiation including UVA, UVB and visible light monitored by agarose gel electrophoresis, (iii) antioxidant activity (ability to scavenge the free radicals 1,1-diphenyl-picrylhydrazyl (DPPH) and 2,2′-azinobis-(3-ethylbenzothiazoline-6-sulfonic acid) (ABTS) and to reduce H_2O_2), and (iv) affinity (calculation of binding constant and determination of the binding site location) for bovine serum albumin (BSA) examined *in vitro* by fluorescence emission spectroscopy.

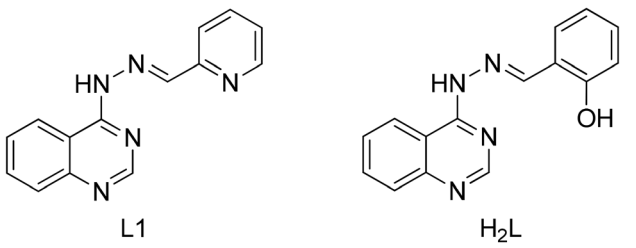

Fig. 1 The syntax formula of (*E*)-4-(2-((pyridin-2-yl)methylene)hydrazinyl)quinazoline (**L1**) and (*E*)-2-((2-(quinazolin-4-yl)hydrazono)methyl) phenol (**H_2L**).

2 Experimental

2.1 Materials – instruments – physical measurements

All chemicals and solvents were reagent grade and were used as purchased from commercial sources; *i.e.* 2-aminobenzonitrile from Fluorochem; ammonium acetate, triethyl orthoformate, hydrazine hydrate, *p*-toluenesulfonic acid monohydrate, salicylaldehyde, CT DNA, EB, BSA, ABTS, $K_2S_2O_8$, nordihydroguaiaretic acid (NDGA), butylated hydroxytoluene (BHT) from Sigma-Aldrich Co; 6-hydroxy-2,5,7,8-tetramethylchromane-2-carboxylic acid (trolox) from J&K sodium warfarin, ibuprofen, DPPH from TCI; $Zn(NO_3)_2\cdot 6H_2O$, $CuCl_2\cdot 2H_2O$, trisodium citrate dihydrate, NaCl, NaH_2PO_4 from Merck; supercoiled circular pBR322 plasmid DNA from New England Bioline; Tris base, boric acid, EDTA disodium salt dehydrate, loading buffer and H_2O_2 (30% w/v) from PanReac Applichem; L-ascorbic acid, Na_2HPO_4 and all solvents from Chemlab. All reactions were monitored on commercially available pre-coated TLC plates (layer thickness 0.25 mm) of Kieselgel 60 F_{254}. Yields were calculated after recrystallization.

CT DNA stock solution was prepared by dilution of CT DNA in buffer (containing 150 mM NaCl and 15 mM trisodium citrate at pH 7.0) followed by exhaustive stirring at 4 °C for 2 days and kept at 4 °C for no longer than a week. The stock solution of CT DNA gave a ratio of UV absorbance at 260 and 280 nm (A_{260}/A_{280}) of ~1.86, indicating that the DNA was sufficiently free of protein contamination.[48] The DNA concentration per nucleotide was determined by the UV absorbance at 260 nm after 1 : 20 dilution using $\varepsilon = 6600\ M^{-1}\ cm^{-1}$.[49]

Infrared (IR) spectra (400–4000 cm^{-1}) were recorded on a Nicolet FT-IR 6700 spectrometer with samples prepared as KBr pellets (abbreviation used: s = strong, vs = very strong, br = broad, m = medium, w = weak) (Fig. S1†). UV-visible (UV-vis) spectra were recorded as nujol mulls and in solution at concentrations in the range 50 μM–5 mM on a Hitachi U-2001 dual beam spectrophotometer. C, H and N elemental analyses were carried out on a PerkinElmer 240 B elemental analyzer. ^{1}H NMR spectra were recorded on an Agilent 500/54 (500 MHz) spectrometer using DMSO-d_6 as solvent. Chemical shifts (δ) are given in ppm and J values in Hz using solvent as an internal reference (abbreviation used: s = singlet, d = doublet, br = broad). Molar conductivity measurements were carried out in 1 mM DMSO solution of the complexes with a Crison Basic 30 conductometer. Fluorescence spectra were recorded in solution on a Hitachi F-7000 fluorescence spectrophotometer. Viscosity experiments were carried out using an ALPHA

L Fungilab rotational viscometer equipped with an 18 mL LCP spindle and the measurements were performed at 100 rpm.

2.2 Synthesis of the compounds

2.2.1 Synthesis of (*E*)-2-((2-(quinazolin-4-yl)hydrazono) methyl)phenol (H_2L). The synthesis of the compound[44] was conducted in three steps including, the synthesis of the 4-aminoquinazoline (**I**) and quinazolin-4-yl-hydrazine (**II**) as intermediates. The synthesis of intermediates **I** and **II** (Scheme 1) has been previously described in ref. 43. In an ethanolic solution of quinazolin-4-yl-hydrazine (**II**) (335 mg, 2.02 mmol), salicylaldehyde (223 μL, 2.09 mmol) was added slowly with continuous stirring in the presence of *p*-toluenesulfonic acid as catalyst. The reaction mixture was refluxed at 90 °C for 3 h. The reaction was monitored by TLC. The reaction mixture was slowly allowed to cool to ambient temperature. Yellow crystalline product suitable for X-ray structure determination precipitated (yield 72%, 394 mg), and was collected by filtration. The product was washed with cold ethanol and dried *in vacuo*. HRMS (ESI) *m*/*z* calc. for $C_{15}H_{13}N_4O^+$: 265.1084 $[M + H]^+$; found 265.1082. ^{1}H NMR (500 MHz, DMSO-d_6, ppm) (Fig. S2†): δ = 11.62 (s, 1H), 10.30 (s, 1H), 8.74 (d, J = 7.4 Hz, 1H), 8.20 (d, J = 7.5 Hz, 1H), 7.92–7.77 (m, 2H), 7.66 (brs, 1H), 7.50 (brs, 1H), 7.42 (brs, 1H), 7.30 (t, J = 7.5 Hz, 1H), 6.97–6.88 (m, 2H). IR (KBr disk), ν (cm^{-1}): 3413 (w) ν(O–H)$_{phenol}$ + ν(N–H)$_{secondary}$; 1630 (vs), 1619 (vs) ν(C═N); 1483 (m) ν(C–C)$_{aromatic}$; 770 (m) w(N–H). UV–vis (DMSO, nm (M^{-1} cm^{-1})): $\lambda_{max}(\varepsilon)$ = 453 (1600), 402 (shoulder(sh)) (5240), 379 (8200), 361 (sh) (740), 288 (4500).

2.2.2 Synthesis of $[Zn(HL)_2]\cdot1.5\ CH_3OH\cdot H_2O$, complex 1. A methanolic solution of KOH (6.34 mg, 0.113 mmol) was added into a methanolic solution (10 mL) of H_2L (30 mg, 0.113 mmol) and the reaction solution was stirred for 1 h. The solution was added dropwise into a warm methanolic solution (5 mL) of $Zn(NO_3)_2\cdot6H_2O$ (15 mg, 0.057 mmol). The reaction mixture was stirred for 30 min, 1 mL of H_2O was added, and the solution was left to evaporate slowly in room temperature. After 5 days, yellow needle-like single-crystals (27 mg, 65%) suitable for X-ray structure determination were deposited and collected by filtration. Elemental analysis calcd for $[Zn(HL)_2]\cdot1.5CH_3OH\cdot H_2O$ ($C_{31.5}H_{30}N_8O_{4.5}Zn$, MW = 658.02): C 57.50, H 4.60, N 17.03; found: C 57.65, H 4.49, N 16.86%. IR (KBr disk), ν (cm^{-1}): 1619 (vs), 1600(s) ν(C═N); 1473 (s) ν(C–C)$_{aromatic}$; 751 (m) w(N–H); 552 (m) ν(M–N); 495 (m) ν(M–O). UV–vis (nujol, nm): λ_{max} = 450, 425, 397; (DMSO, nm (M^{-1} cm^{-1})): $\lambda_{max}(\varepsilon)$ = 449 (1200), 423 (1500), 401 (1300), 380 (1050), 359 (1350), 341 (7500), 290 (7200). The complex is soluble in DMSO (Λ_M = 9 S cm^2 mol^{-1}, 1 mM in DMSO).

2.2.3 Synthesis of $[Cu_4(L)_4(DMF)_4]\cdot8H_2O$, complex 2. A methanolic solution of KOH (8.5 mg, 0.152 mmol) was added into a DMF solution (8 mL) of H_2L (20 mg, 0.076 mmol). After 1 h stirring, the solution was added dropwise into a DMF solution (2 mL) of $CuCl_2\cdot2H_2O$ (6.4 mg, 0.0378 mmol). The solution was stirred at 50 °C for 15 min and was left to cool and evaporate at room temperature. Green single-crystals (35 mg, 50%) suitable for X-ray structure determination were deposited after two months and were collected. Elemental analysis calcd for $[Cu_4(L)_4(DMF)_4]\cdot8H_2O$, ($C_{72}H_{84}Cu_4N_{20}O_{16}$, MW = 1739.77): C 49.71, H 4.87, N 16.10; found: C 49.55, H 4.74, N 15.90%. IR (KBr disk), ν (cm^{-1}): 1628 (vs) ν(C═N); 1471 (m) ν(C–C)$_{aromatic}$; 750 (m) w(N–H); 560 (m) ν(M–N); 495 (w) ν(M–O). UV–vis: (nujol, nm): λ_{max} = 615, 445, 415, 395; (DMSO, nm (M^{-1} cm^{-1})): $\lambda_{max}(\varepsilon)$ = 610 (160), 443 (1850), 419 (9900), 391 (5100), 360 (3700), 343 (3000), 275 (11 500). The complex is soluble in DMSO (Λ_M = 11 S cm^2 mol^{-1}, 1 mM in DMSO).

2.3 X-ray crystal structure determination

Suitable single-crystals of the compounds were mounted on thin glass fibers with the aid of epoxy resin. X-ray diffraction data were recorded on a Bruker Apex II CCD area-detector diffractometer, equipped with a Mo Kα (λ = 0.71073 Å) sealed tube source and a Triumph monochromator at 295 K, using the φ and ω scans technique. The program Apex2 (Bruker AXS, 2006) was used for data collection and cell refinement. The collected data were integrated with the Bruker SAINT software package,[50] using a narrow-frame algorithm. Data were corrected for absorption using the numerical method SADABS,[51] based on the crystal dimensions. Structures were solved using the SUPERFLIP package[52] and refined with full-matrix least-squares on F^2 using the Crystals program package version 14.61 build 6236.[53] Anisotropic displacement parameters were applied all non-hydrogen non disordered atoms of the complexes and the non-disordered solvent atoms, while hydrogen atoms were in general found and/or positioned geometrically and refined using a riding model. All disordered atoms (water solvate molecules and coordinated DMF) were isotropically

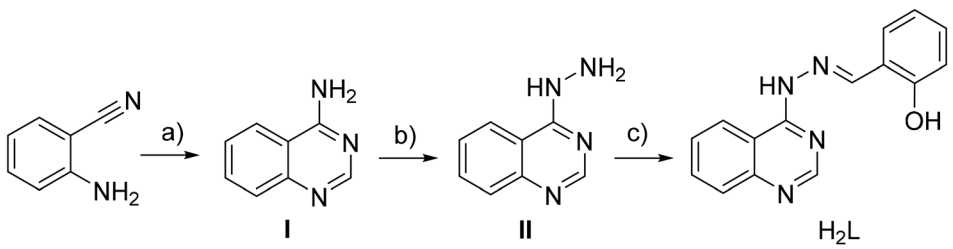

Scheme 1 Synthesis of compound H_2L. (a) NH_4OAc, $HC(OEt)_3$, EtOH reflux, 3.5 h, 78% yield; (b) NH_2NH_2, reflux, 24 h, 53% yield; (c) salicylaldehyde, *p*-TsOH, EtOH reflux, 3 h, 72% yield.

refined with fixed occupation factors. Details of crystal data and structure refinement parameters are shown in Table S1.†

2.5 Study of the biological profile of the compounds

All the procedures and relevant equations used in the *in vitro* study of the biological activity (antioxidant activity, and interaction with CT DNA, plasmid DNA and BSA) of the compounds can be found in the ESI file (sections S1–S4†).

3 Results and discussion

3.1 Synthesis and characterization

The synthesis of compound **H_2L** was performed in three steps (Scheme 1). The synthesis of 4-aminoquinazoline (step I) and quinazolin-4-yl-hydrazine (step II) has been previously reported.[40–43] Quinazolin-4-yl-hydrazine (compound **II**) reacted with salicylaldehyde to give in high yield (72%) (*E*)-2-((2-(quinazolin-4-yl)hydrazono)methyl)phenol (**H_2L**). The data obtained for the known compounds **I** and **II** were in full accordance with the literature reported.[40–43] Compound **H_2L** was fully characterized by IR, ^{1}H NMR, HRMS and UV-vis spectroscopies (Fig. S1–S3†) and single-crystal X-ray crystallography.

The complexes were prepared *via* the aerobic reaction of a solution deprotonated quinazoline with the corresponding metal salts of Zn(II) and Cu(II). The reaction of Zn(II) with deprotonated quinazoline (HL^{-1}) in a 1 : 2 Zn(II) : HL^{-1} ratio resulted in complex **1**, while the reaction of Cu(II) with doubly deprotonated (L^{-2}) in a 1 : 1 Cu(II) : L^{-2} ratio led to the formation of complex **2**. The coordination compounds were characterized by IR and UV-vis spectroscopies, and single-crystal X-ray crystallography.

The complexes are stable in air, soluble in DMSO and insoluble in H_2O. The molar conductivity values of the complexes were recorded in a 1 mM DMSO solution. Both complexes bear Λ_M values in the range 9–11 S cm^2 mol^{-1} showing their non-electrolytic nature[54] which is in accordance with the formulas found from single-crystal X-ray crystallography.

The FT-IR spectra of the compounds (Fig. S1†) are complicated due to the presence of the phenol and quinazoline groups. The IR spectrum of **H_2L** shows a weak band at 3413 cm^{-1} which can be assigned to the ν(O–H)$_{phenol}$ and the ν(N–H) group and intense bands at 1630 cm^{-1} and 1619 cm^{-1} which can be associated with the hydrazone ν(C=N) group.[40–43] In the IR spectra of compounds **1** and **2**, these bands have shifted slightly suggesting the formation of the complexes.[55] The formation of the complexes may be also verified by the appearance of medium-intensity bands in the regions 552–560 cm^{-1} and 494–495 cm^{-1} which can be assigned to ν(M–N) and ν(M–O), respectively.[40–42]

The UV-vis spectra of the compounds (Fig. S3†) were recorded in DMSO solution and as nujol mull. The UV-vis spectra of both complexes in solid state (nujol) showed similar patterns with those recorded in DMSO solution; therefore, their stability in solution may be proposed. In these spectra, the bands observed in the UV or near-UV region of the spectrum located at 270–290 nm and 350–453 nm may be attributed to intra-ligand transitions, typical to C=N and C=C bonds. In the spectra of the complexes, these bands are shifted indicating the formation of the complex. In particular, the band of **H_2L** at 379 nm which is related to the hydrazone group suffered a bathochromic shift in the UV-vis spectra of the complexes. In addition, the bands located at 400–453 nm may be attributed to charge-transfer transitions. In the visible region of the spectrum of complex **2**, the band observed at 610 nm (ε = 160 M^{-1} cm^{-1}) is attributed to a d-d transition and is typical for a square pyramidal geometry for copper(II) complexes.[56]

3.2 Structure of the compounds

The structures of all three compounds were determined by single-crystal X-ray crystallography.

3.2.1 Structure of H_2L. The compound crystallized in orthorhombic crystal system and *Pbca* space group (Table S1†). The molecular structure is depicted in Fig. 2 and selected bond lengths and angles are summarized in Table S2.†

It should be noted that almost all atoms seem to be coplanar, since all three aromatic rings are lying in the same plane with slight deviations. Hydrogen-bonds contribute to the stabilization of the structure (Table S3†). More specifically, an intramolecular hydrogen-bond is formed between the phenolic hydrogen H11 and hydrazine N4, and an intermolecular hydrogen-bond exists between H12 of the quinazoline nitrogen N1 and quinazoline N2^i of an adjacent molecule.

3.2.2 Structure of complex $[Zn(HL)_2]\cdot 1.5CH_3OH\cdot H_2O$. The compound crystallized in monoclinic crystal system and $P2_1/n$ space group (Table S1†). The molecular structure is depicted in Fig. 3 and selected bond lengths and angles are summarized in Table S4.†

The asymmetric unit comprises two crystallographically independent neutral mononuclear Zn(II) complexes, notated as complex **1A** and **1B**, as well as three methanol and one water solvate molecules. Both **H_2L** ligands in each complex act as monoanions (HL^-) after deprotonation of the phenolic hydrogen atom. All ligands are coordinated to Zn(II) in a tridentate fashion through two nitrogen atoms – coming one from the quinazoline and one from the hydrazine parts – and the phenolate oxygen, *i.e.* in complex **1A** N1, N4 and O1 for the

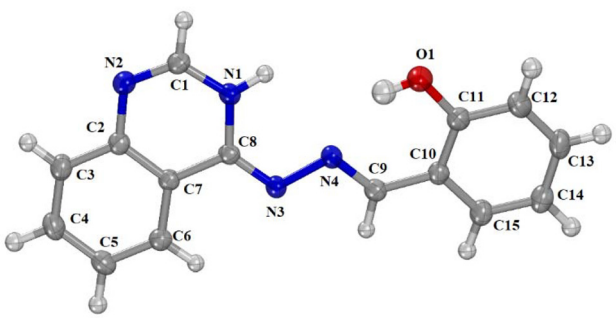

Fig. 2 The molecular structure of H_2L.

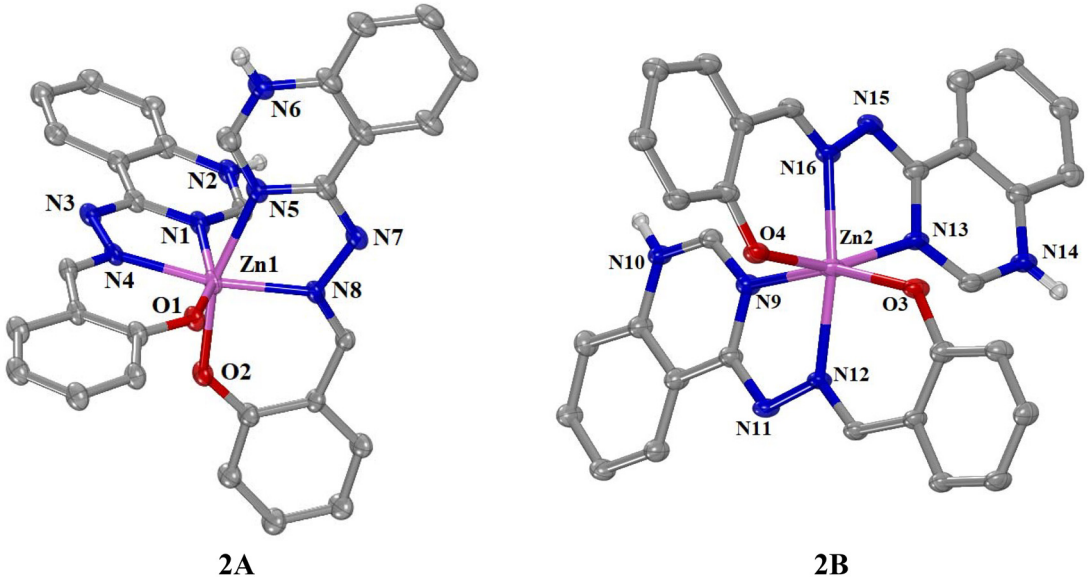

Fig. 3 The molecular structure of complex **1A** and **1B**. The C-bonded hydrogen atoms and solvate molecules are omitted for clarity reasons.

first ligand and N5, N8 and O2 for the second ligand respectively. This coordination mode leads to the formation of two fused chelate rings for each ligand, a five- and a six-membered one and gives rise to a six-coordinated Zn(II) cation with a N_4O_2 environment. In both complexes, the resulting disordered coordination octahedron has as most axial vector the $N_{hydrazone}$–Zn–$N_{hydrazone}$ containing nitrogen atoms forming angles *i.e.* N4–Zn1–N8 = 165.41(10)° for complex **1A** and N12–Zn2–N16 = 164.29(10)° for **2A**.

A series of intermolecular H-bonds between adjacent molecules of the complexes and with solvate molecules result in further stabilization of the structure (Table S3†).

3.2.3 Structure of complex $[Cu_4(L)_4(DMF)_4]\cdot 8H_2O$, complex 2. The complex crystallized in tetragonal crystal system and $I4_1/a$ space group (Table S1†). The molecular structure is shown in Fig. 4 and selected bond distances and angles are given in Table S5.†

Complex **2** is a neutral tetranuclear copper(II) complex consisting of four Cu(II) ions, four doubly deprotonated L^{2-} ligands and four DMF ligands, while there are also eight solvate water molecules. In the complex, the four doubly deprotonated quinazoline ligands (L^{2-}) are coordinated to Cu(II) ions in a tetradentate bridging manner. More specifically, the quinazoline nitrogen atom N1, the hydrazine nitrogen atom N4, and the phenolate oxygen atom O1 are coordinated to Cu1, leading to the formation of two fused chelate rings, a five- and a six-membered one. The coordination sphere of the pentacoordinate Cu(II) ion is completed by the deprotonated quinazoline nitrogen atom $N2^i$ of an adjacent ligand and the oxygen atom O2 of the DMF ligand. According to the value of the trigonality index τ_5 = 0.10 (=(175.9° − 169.9°)/60°, $\tau_5 = (\varphi_1 - \varphi_2)/60°$, φ_1 and φ_2 are the largest angles in the coordination sphere;[57] τ_5 = 0 is found for a perfect square pyramid and τ_5 = 1 for a perfect trigonal bipyramid), the geometry around each Cu(II) ion can be described as slightly distorted square pyramid with O1, N1, N4 and $N2^i$ atoms forming the basal plane and O2 being at the apical of the pyramid.

The four Cu(II) ions are bridged by four L^{2-} ligands *via* the quinazoline atoms N1–C1–N2 creating a 16-membered saddle-like azametallacoronate (azaMCor) ring of the type [16-azaMCor-4] with a [–N–C–N–Cu–] repeating unit. To the best of our knowledge,[22–27,35–37] complex **2** is among the very few examples of an azametallacoronate compound of the type [16-azaMCor-4] reported.[39] The interatomic distances between the neighboring Cu(II) ions (Cu1···$Cu1^i$) and the non-neighboring Cu(II) ions (Cu1···$Cu1^{ii}$) are 5.797 Å and 6.574 Å, respectively. Similar arrangement of the Cu(II) ions was also observed in a series of [16-MCor-4] metallacoronates of the formula $[Cu_4(carboxylato)_4(X)_4]$ (X = Cl^-, ClO_4^-).[35,38] The arrangement of the four Cu(II) participating in the azametallacoronate ring results in the formation of a hollow space in the [16-azaMC-4] ring where four DMF ligands are encapsulated. Each DMF ligand is coordinated to a ring Cu(II) ion *via* its oxygen atom O2 orientated towards the center of the [16-azaMC-4] (Fig. 4).

The extended hydrogen-bonded system involving the solvate water molecules as well as the π–π stacking interactions between the ligands from neighboring complexes offer further stabilization of the structure (Table S3†).

3.3 Interaction with DNA

3.3.1 Affinity for CT DNA. The interaction of the compounds with CT DNA was investigated by UV-vis spectroscopy, DNA-viscosity titrations, and *via* competitive studies with EB which were monitored by fluorescence emission spectroscopy.

Titration studies using UV-vis spectroscopy were employed in order to investigate the interaction of the compounds with CT DNA and the strength of this interaction by calculating the corresponding DNA-binding constant (K_b). Within this

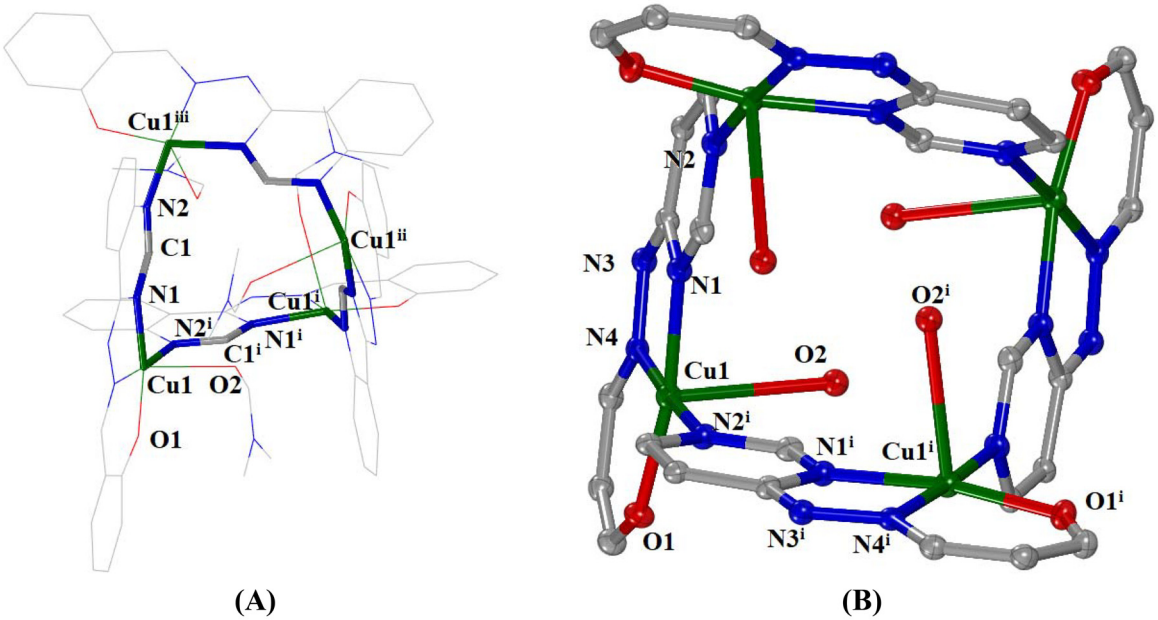

Fig. 4 The molecular structure of complex **2** (A) highlighting the metallacoronate ring (in bold) and (B) showing the coordination spheres of Cu(II) ions. The hydrogen atoms and solvate H_2O molecules are omitted for clarity reasons. Symmetry codes: (i) $-y + 5/4, x + 1/4, -z + 5/4$; (ii) $y - 1/4, -x + 5/4, -z + 5/4$.

context, initially the UV-vis spectra of a CT DNA solution in buffer were recorded in the presence of $\mathbf{H_2L}$ or complexes **1** and **2** at diverse ratios of [compound]/[DNA] (= *r*). Upon addition of increasing amounts of the compounds, a slight change of the absorbance (either hypochromism or hyperchromism) of the CT DNA band located at λ_{max} = 258–260 nm was observed (Fig. S4†) indicating the existence of an interaction.

On the reverse titrations, the UV-vis spectra of the compounds were recorded upon addition of increasing amounts of CT DNA and a series of changes of the charge-transfer or intraligand band(s) of the compounds were observed (Fig. 5(A), and S5† and Table 1). The overall changes of these bands were rather complicated showing hypochromism and/or hyperchromism which may be accompanied by slight blue- or red-shift (Table 1). The features in the UV spectra of CT DNA confirmed the interaction between the compounds and CT DNA suggesting the formation of a new adduct between CT DNA and the compound. Because of the complicated UV spectra of

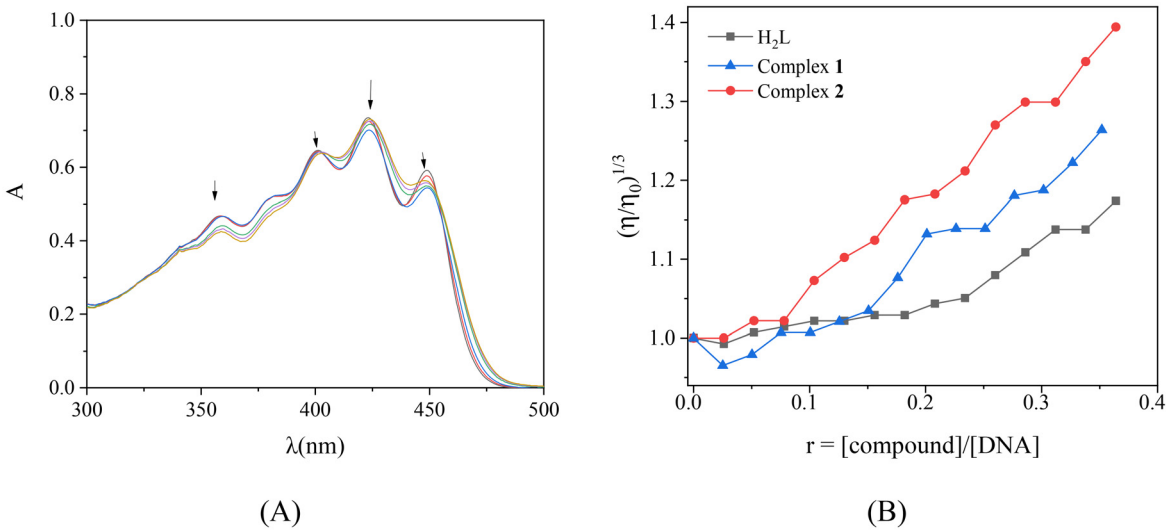

Fig. 5 (A) UV-vis spectra of a DMSO solution of complex **1** (0.05 mM) in the presence of increasing amounts of CT DNA. The arrows show the changes upon increasing amounts of CT DNA. (B) Relative viscosity $(\eta/\eta_0)^{1/3}$ of CT DNA (0.1 mM) in buffer solution (150 mM NaCl and 15 mM trisodium citrate at pH 7.0) in the presence of $\mathbf{H_2L}$ and its complexes **1** and **2** at increasing amounts (*r* = [complex]/[DNA]).

Table 1 UV–vis spectral features of H_2L and its complexes **1** and **2** with CT DNA

Compound	λ (nm) ($\Delta A/A_0$ [a] (%), $\Delta\lambda$ [b] (nm))	K_b (M^{-1})
H_2L	361(sh)[c] (−12,[a] +1 [b]); 379 (−12,[a] −1 [b]), 401(sh) (+3, −1); 453 (>+50,[d] −10)	2.04(±0.59) × 10^6
Complex **1**	341 (−3, +1); 359 (−9, 0); 380 (−9, −2); 401 (−2, 0); 423 (−5, +1); 449 (−8, 0)	1.44(±0.32) × 10^7
Complex **2**	343 (−3, −1); 360 (−2, −1); 391 (+2, elim[e]); 419 (−9, −2); 443 (−10, −2)	8.38 (±0.50) × 10^6

UV-band (λ, in nm) (percentage of the observed hyper-/hypo-chromism ($\Delta A/A_0$, in %), blue-/red-shift of the λ_{max} ($\Delta\lambda$, in nm)) and DNA-binding constants (K_b, in M^{-1}). [a] "+" denotes hyperchromism, "−" denotes hypochromism. [b] "+" denotes red-shift, "−" denotes blue–shift. [c] sh = shoulder. [d] >+50 denotes high hyperchromism. [e] elim = eliminated.

the compounds bearing so many transition bands, it is not easy to suggest a discrete mode of DNA-binding and more studies such as DNA-viscosity measurements and competitive studies with EB were conducted to reach a safer conclusion regarding the interaction mode.

The Wolfe–Shimer equation (eqn (S1)†)[58] and the plots [DNA]/($\varepsilon_A - \varepsilon_f$) *versus* [DNA] (Fig. S6†) were used for the calculation of the K_b values of the compounds. All three compounds presented significantly high DNA-binding constants which were higher than that of the classic intercalator EB (= 1.23 × 10^5 M^{-1}).[59] Both complexes exhibit high DNA-affinity than H_2L (Table 1) with complex **1** showing the highest DNA-binding constant (K_b = 1.44(±0.32) × 10^7 M^{-1}) among the compounds. A comparison of the K_b values derived for the compounds with reported compounds bearing a series of pyridine analogues of H_2L, *i.e.* (*E*)-4-(2-(pyridin-2-ylmethylene)hydrazinyl)quinazoline and its halogenated derivatives,[40–43] may reveal that the existence of the phenol ring in H_2L resulted in higher affinity for CT DNA.

The viscosity of DNA-solution was examined because DNA-viscosity is sensitive to changes in the relative DNA chain-length making viscometry a useful method to clarify the DNA-interaction mode. The viscosity of a CT DNA solution (0.1 mM) was measured in the presence of incrementally increasing amounts of compounds (up to r = [compound]/[DNA] = 0.36). For all compounds, the viscosity increased significantly (Fig. 5(B)) suggesting intercalation as the most possible mode of their interaction with CT DNA; the increase of relative DNA-viscosity is related to increase of the relative DNA-length as a result from the increase of the distance between DNA-bases due to intercalation of the inserting compounds.[60,61] A slight lowering of DNA-viscosity was also observed at the early steps of incremental addition of H_2L and complex **1** (for r values up to 0.10), indicating an initial external interaction resulting in closer approach which was followed by intercalation.

The planar phenanthridine ring of the typical DNA-intercalator EB inserts in-between two adjacent DNA-bases resulting in an intense fluorescence emission band at 592–594 nm upon excitation of the solution at 540 nm. In order to explore the potential intercalation effect of the compounds, the fluorescence emission spectra of a solution containing EB-DNA (after 1–h pretreatment of EB (40 μM) and CT DNA (40 μM) in buffer solution) were recorded in presence of increasing amounts of solution of the compounds. The addition of the compounds in the EB-DNA solution led to a quenching of the fluorescence emission band at 594 nm (representatively shown for complex **2** in Fig. 6(A)). The quenching was significant (up to ~69% of the initial fluorescence, Table 2 and Fig. 6(B)), and may be assigned to the displacement of EB from the EB-DNA adduct.[62]

The quenching ability of the compounds can be evaluated through the values of the Stern–Volmer constant (K_{SV}) and

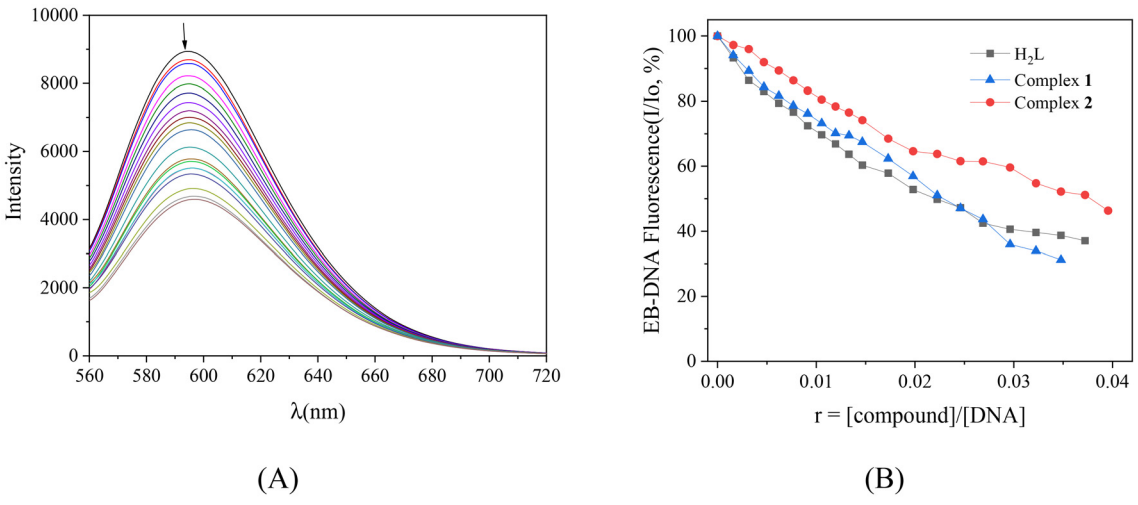

Fig. 6 (A) Fluorescence emission spectra ($\lambda_{excitation}$ = 540 nm) for EB-DNA conjugate ([EB] = 40 μM, [DNA] = 40 μM) in buffer solution (150 mM NaCl and 15 mM trisodium citrate at pH = 7.0) in the absence and presence of increasing amounts (up to r = [complex]/[DNA] = 0.04) of complex **2**. The arrow shows the changes of intensity upon increasing amounts of the complexes. (B) Plot of EB-DNA relative fluorescence emission intensity at $\lambda_{emission}$ = 592 nm (I/I_0, %) *versus* r (r = [complex]/[DNA]) in the presence of H_2L and its complexes **1** and **2** (up to 37.1% of the initial EB-DNA fluorescence emission intensity H_2L, 31.2% for **1**, and 46.3% for **2**).

Table 2 Fluorescence features of the EB-displacement studies of H_2L and its complexes **1** and **2**

Compound	$\Delta I/I_0$ (%)	K_{SV} (M^{-1})	k_q (M^{-1} s^{-1})
H_2L	62.9	$7.67(\pm0.15) \times 10^5$	$3.34(\pm0.06) \times 10^{13}$
Complex **1**	68.8	$3.65(\pm0.14) \times 10^5$	$1.59(\pm0.06) \times 10^{13}$
Complex **2**	53.7	$4.22(\pm0.09) \times 10^5$	$1.84(\pm0.04) \times 10^{13}$

Percentage of EB-DNA fluorescence emission quenching ($\Delta I/I_0$, in %), Stern–Volmer constants (K_{SV}, in M^{-1}) and quenching constants (k_q, in M^{-1} s^{-1}).

quenching constant (k_q) which were calculated with the Stern–Volmer equations (eqn (S2) and (S3)† after using the value of 23 ns as the fluorescence lifetime of EB-DNA system (τ_0)),[63] and the corresponding Stern–Volmer plots (Fig. S7†). The K_{SV} values of the compounds are relatively high (Table 2) and are similar with reported compounds bearing pyridine analogues of **H_2L**.[40–43] In addition, the quenching constants are of the order 10^{13} M^{-1} s^{-1} (Table 2) and are three orders higher than the value of 10^{10} M^{-1} s^{-1}, suggesting the existence of a static quenching mechanism which may confirm the formation of a new adduct between DNA and each complex.[62]

3.3.2 Interaction of the compounds with plasmid DNA. In the attempt to investigate the nuclease-like activity of the compounds, the cleavage and photocleavage of pBR322 plasmid DNA (pDNA) by them was monitored *via* agarose gel electrophoretic experiments. For this purpose, DMSO solutions (500 μM, DMSO within the final mixture never exceeded 10% v/v) of the compounds (**H_2L**, complexes **1** and **2**) were mixed with pBR322DNA (tris buffer solution, 25 μM, pH = 6.8). Four experiments have been performed with plasmid DNA and the results were analyzed by gel electrophoresis on 1% agarose stained with EB: (i) in dark upon incubation of the components for 150 min (Fig. S8(A)†); (ii) upon irradiation at 312 nm (UV-B) for 30 min (Fig. S8(B)†); (iii) upon irradiation at 365 nm (UV-A) for 120 min (Fig. S8(C)†) and (iv) upon irradiation under visible light for 120 min (Fig. S8(D)†). The supercoiled pDNA in an agarose gel during electrophoresis is shown as Form I (Fig. S8,† lane 1). For the photocleavage experiments all compounds have been incubated with pDNA for 30 min at 37 °C prior to irradiation. Dark control experiments have been performed upon incubation of the compounds with pDNA for 150 min, in order to cover incubation time (30 min) and the 120 min of incubation of the samples which were irradiated-total incubation time 150 min.

The potential DNA-cleaving activity of the compounds was quite negligible upon lack of irradiation (Fig. S8(A)†) or upon irradiation at 312 nm (Fig. S8(B)†). In all experiments, complex **1** proved incapable of cleaving or photocleaving pDNA. In some cases, *i.e.* for **H_2L** upon irradiation at 365 nm (Fig. S8 (C)†) and for complex **2** upon irradiation with UVA (Fig. S8(C)†) and visible light (Fig. S8(D)†), the pDNA-cleavage was revealed only as single-stranded (ss) nicks in the supercoiled DNA forming relaxed circular DNA (Form II), while no signal (double-stranded (ds) nick) attributed to the formation of linear DNA (Form III) was observed. For these cases, the percentages of the cleavage (shown in Fig. S8†) were calculated with eqn (S4) and (S5).† At the high concentration of 500 μM used in the experiment, these compounds present rather low-to-negligible ability to cleave DNA with complex **2** showing the highest photocleavage activity of 10% (Fig. S8(D),† lane 4).

The lack of pDNA-cleavage activity of the herein reported compounds, when compared to a series of metal complexes bearing (*E*)-4-(2-(pyridin-2-ylmethylene)hydrazinyl)quinazoline[40–43] and its halogenated derivatives as ligands (they are the pyridine analogues of **H_2L**), may be possibly attributed to the exchange of the pyridine ring by the phenol ring in **H_2L** which results to formation of anionic ligands and six-membered chelate rings when coordinated to metal(II) ions.

3.4 Antioxidant activity of the compounds

Taking into consideration that compounds with antioxidant properties might play an important role in the development of effective pharmaceuticals[64] as well as that anti-inflammatory activity has been reported for a series of quinazoline derivatives,[65,66] the potential antioxidant activity of the compounds was assessed through monitoring their ability to scavenge DPPH and ABTS free radicals and to reduce H_2O_2. The results are summarized in Table 3, and the activities were compared with the activity of well-known reference compounds NDGA, BHT, trolox and L-ascorbic acid.[64,67,68]

The neutralization of DPPH radicals by potential antioxidants is often related with potential activity against cancer, aging process and/or inflammation.[64] The ability of the compounds to scavenge DPPH radicals was time-independent, as shown after measuring the absorbance after 30-min and 60-min reaction. Complex **2** was proved inactive towards DPPH radicals while **H_2L** and complex **1** showed quite low scavenging activity (up to 10.36 ± 0.19%), especially when compared with the reference compounds NDGA and BHT (Table 3).

The activity of the compounds towards the cationic ABTS radicals (the ABTS-scavenging is related to the overall antioxidant activity of compounds) is more enhanced (up to 71.63 ± 0.94% for complex **1**) when compared to DPPH but still lower than the activity of the corresponding reference compound trolox (Table 3).

The scavenging or the reduction of hydrogen peroxide is related to the relief from oxidative stress and/or inhibition of reactive oxygen species.[69] The interaction of the compounds

Table 3 %DPPH-scavenging ability (DPPH%), %ABTS radical scavenging activity (ABTS%) and H_2O_2-reducing ability (H_2O_2%) for the compounds

Compound	DPPH% 30 min	DPPH% 60 min	ABTS%	H_2O_2%
H_2L	6.52 ± 0.12	7.98 ± 0.17	54.73 ± 1.56	87.98 ± 0.46
Complex **1**	9.54 ± 0.42	10.36 ± 0.19	71.63 ± 0.94	60.59 ± 0.47
Complex **2**	Inactive	Inactive	19.97 ± 1.32	67.76 ± 0.74
NDGA	87.08 ± 0.12	87.47 ± 0.12	Not tested	Not tested
BHT	61.30 ± 1.16	76.78 ± 1.12	Not tested	Not tested
Trolox	Not tested	Not tested	98.0 ± 0.48	Not tested
L-Ascorbic acid	Not tested	Not tested	Not tested	60.80 ± 0.48

with H_2O_2 revealed that the complexes are less active (H_2O_2% = 60.59–67.76%, Table 3) than free **H_2L** (87.98 ± 0.46%). However, all compounds present equal or better activity than the reference compounds L-ascorbic acid (= 60.80 ± 0.20%).

The overall antioxidant behavior of the compounds is rather poor towards DPPH radicals, moderate towards ABTS radicals and significant towards H_2O_2. Such antioxidant profile is in accordance with the results reported for compounds containing the pyridine analogues of **H_2L**.[40–43]

3.5 Interaction of the compounds with BSA

3.5.1 Affinity of the compounds for BSA. The interaction of the compounds with BSA was investigated as a means to monitor whether the compounds under study have the potency to bind to BSA in order to get transferred to their potential biotargets. The two main roles of the abundant protein in bloodstream, serum albumin, are the maintenance of the osmotic pressure (which is important for the maintenance of cells and tissues) and the transportation of bioactive compounds.[70] BSA is the most extensively studied albumin and is structurally similar to human serum albumin possessing two tryptophan residues at positions 134 and 212. The interaction was studied by fluorescence emission quenching experiments.[62]

The fluorescence emission spectra of a BSA solution (3 mM) were recorded in the range 300–500 nm for $\lambda_{excitation}$ = 295 nm in the presence of incrementally increasing amounts of the compounds (up to r = [compound]/[BSA] = 6.2). The initial BSA emission band with $\lambda_{max,\ emission}$ at 343 nm showed upon addition of the compounds a significant decrease with complex **2** inducing the highest percentage (>97%) of the BSA quenching (Fig. 7). The observed quenching can be assigned to re-arrangement or modifications of the SA secondary structure which may result from the association of the compounds with BSA.[62] The influence of the inner-filter effect on the measurements was calculated with eqn (S6)†[71] and it was too negligible to affect the measurements.

The Stern–Volmer constants (K_{SV}), the BSA-quenching constants (k_q) and the BSA-binding constants (K) of the compounds were calculated with the Stern–Volmer and Scatchard equations (eqn (S2), (S3) and (S7)†) and plots (Fig. S9 and S10†) applying the value of 10^{-8} s as the fluorescence lifetime of tryptophan in SAs (τ_0).[62] The calculated k_q values of the compounds are significantly higher (in most cases by three-to-four orders) than the value of 10^{10} M^{-1} s^{-1} (Table 4) suggesting a static mechanism for the observed quenching,[62] which confirms the interaction of the compounds with BSA.

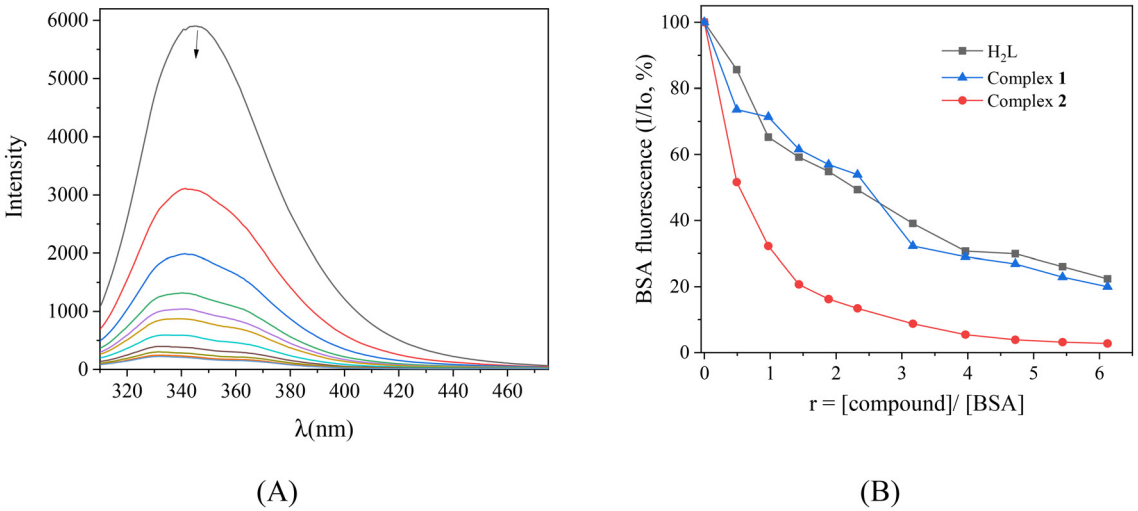

Fig. 7 (A) Fluorescence emission spectra ($\lambda_{excitation}$ = 295 nm) of a buffer solution (150 mM NaCl and 15 mM trisodium citrate at pH 7.0) of BSA (3 μM) in the presence of increasing amounts of complex **2**. The arrow shows the changes of intensity upon increasing amounts of the complex. (B) Plot of % relative fluorescence intensity at λ_{em} = 343 nm (I/I_0, %) *versus* r (r = [complex]/[BSA]) for **H_2L** and its complexes (up to 22.4% of the initial BSA fluorescence for **H_2L**, 20.0% for **1**, and 2.7% for **2**).

Table 4 Fluorescence features of the BSA-binding studies of **H_2L** and its complexes **1** and **2**

Compound	k_q (M^{-1} s^{-1})	$K_{(BSA)}$ (M^{-1})	$K_{(BSA,ibu)}$ (M^{-1})	$K_{(BSA,warf)}$ (M^{-1})
H_2L	$1.84(\pm0.06) \times 10^{13}$	$1.30(\pm0.08) \times 10^{5}$	$2.32(\pm0.03) \times 10^{5}$	$1.32(\pm0.04) \times 10^{5}$
Complex **1**	$2.16(\pm0.09) \times 10^{13}$	$1.05(\pm0.04) \times 10^{5}$	$4.07(\pm0.19) \times 10^{5}$	$3.16(\pm0.09) \times 10^{5}$
Complex **2**	$2.05(\pm0.09) \times 10^{14}$	$5.60(\pm0.18) \times 10^{5}$	$1.17(\pm0.06) \times 10^{6}$	$1.17(\pm0.64) \times 10^{5}$

BSA-quenching constants (k_q, in M^{-1} s^{-1}), and BSA-binding constants (K, in M^{-1}) of the compounds in the absence ($K_{(BSA)}$) or presence of a site-marker warfarin ($K_{(BSA,warf)}$) or ibuprofen ($K_{(BSA,ibu)}$).

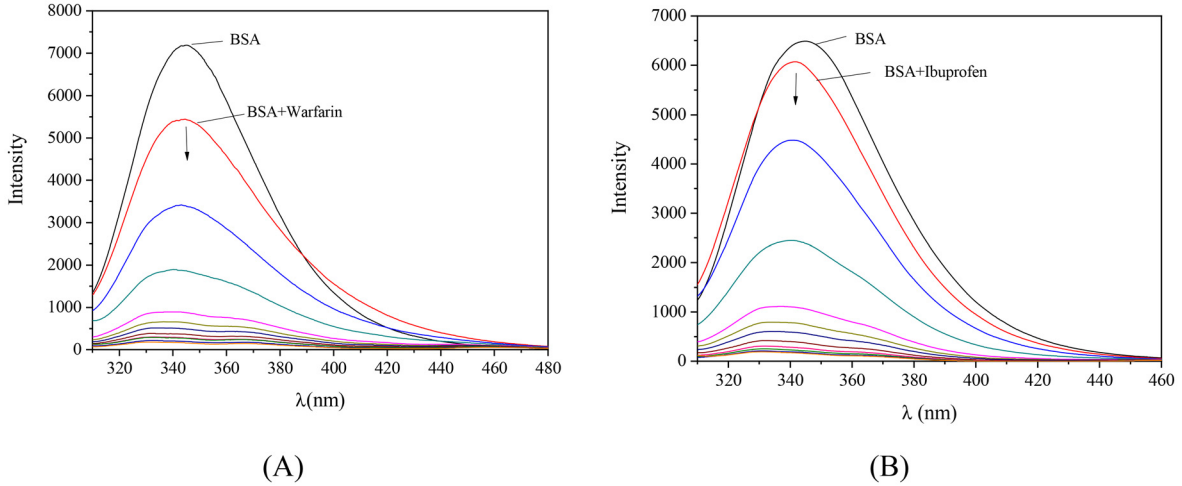

Fig. 8 Fluorescence emission spectra ($\lambda_{excitation}$ = 295 nm) of a buffer solution (150 mM NaCl and 15 mM trisodium citrate at pH 7.0) of BSA (3 μM) in the presence of (A) warfarin (3 μM) or (B) ibuprofen (3 μM), upon addition of increasing amounts of complex **2**. The arrows show the changes of intensity upon increasing amounts of the complexes.

The values of the BSA-binding constants of the compounds are of the order 10^5 M^{-1} (Table 4) with complex **2** showing the highest K value (= 5.60(±0.18) × 10^5 M^{-1}) among the compounds under study. The affinity of the compounds is within the range also reported for the pyridine analogues of $\mathbf{H_2L}$.[40–43] However, the BSA-binding constants found for the compounds observed are lower than the value of 10^{15} M^{-1} which is considered as the limit for reversible noncovalent interactions. Within this context, the BSA-binding constants of the compounds reveal their reversible binding to the BSA in order to get transported and get released upon arrival at their potential biological targets.[72]

3.5.2 Binding site of BSA. The albumin has four sites where drugs and metal ions can be hosted with Sudlow's site 1 (or drug site I) and Sudlow's site 2 (or drug site II) in subdomains IIA and IIIA, respectively, being the most known.[73] In order to recognize the potential BSA-binding site of the compounds, warfarin and ibuprofen are used as common site-markers for Sudlow's site 1 and Sudlow's site 2, respectively.[43,74] Within this context, the BSA-binding constants of the compounds were determined in the presence of the site-markers by fluorescence emission quenching experiments and were compared with those found in the absence of any site-marker (values in Table 4).

The incremental addition of the compounds in a solution containing BSA and the corresponding site-marker (warfarin or ibuprofen) resulted in a significant quenching of the initial fluorescence emission band (Fig. S11 and S12† and representatively shown for complex **2** in Fig. 8). The BSA-binding constants of the compounds were determined with the Scatchard equation (eqn (S7)†) and plot (Fig. S13 and S14†). Any decrease of the BSA-binding constant in the presence of the site-marker will show that the binding of the compound to BSA is influenced by the coexistence of this marker inhibiting the approach of the compound due to the competition for the same binding site.[41,43,74] From the K values shown in Table 4, a safe conclusion concerning a preferable drug site can be given only for complex **2** which showed a significant decrease of the BSA-binding constant in the presence of warfarin indicating its selective binding to Sudlow's site 1 in subdomain IIA.

4 Conclusions

A novel quinazoline ligand containing a phenol ring, namely (*E*)-2-((2-(quinazolin-4-yl)hydrazono)methyl)phenol ($\mathbf{H_2L}$) and its Zn(II) and Cu(II) complexes, $[Zn(HL)_2]\cdot 1.5CH_3OH\cdot H_2O$ (complex **1**) and $[Cu_4(L)_4(DMF)_4]\cdot 8H_2O$ (complex **2**), respectively, were isolated and characterized with spectroscopic techniques and single-crystal X-ray crystallography. In mononuclear complex **1**, the quinazoline derivative is simply deprotonated acting as a tridentate ligand *via* the quinazoline and the hydrazone nitrogen atoms and the deprotonated phenolate oxygen atom. In tetranuclear complex **2**, the doubly deprotonated quinazoline acted as a tetradentate bridging ligand *via* the quinazoline and the hydrazone nitrogen atoms and the deprotonated phenolic oxygen atom to a Cu(II) ion and the second quinazoline nitrogen atom to an adjacent Cu(II) ion. A cyclic 16-membered structure containing four [–N–C–N–Cu–] repeating units is formed and complex **2** is a characteristic [16-azaMCor-4] example among the few reported azametallacoronate compounds.

The potential biological profile of the compounds was evaluated regarding their interaction with biomacromolecules (BSA and DNA), and their antioxidant ability. The compounds may interact with CT DNA *via* intercalation and the highest DNA-binding constant was found for complex **1** (K_b = 1.44(±0.32) × 10^7 M^{-1}). The ability of the

compounds to cleave pBR322 plasmid DNA to relaxed circular DNA was rather low-to-negligible at the high concentration of 500 μM.

The binding of compounds to BSA is tight and reversible, suggesting they can be transported by the albumins and released at potential biotargets. Furthermore, competitive studies with the typical site-markers warfarin and ibuprofen were employed to explore whether the compounds bind selectively to typical BSA-binding sites. A safe conclusion was reached only for complex **2** regarding its selective binding to Sudlow's site 1 in subdomain IIA.

Regarding the antioxidant activity of the compounds, their ability to scavenge DPPH and ABTS free radicals and to reduce H_2O_2 was explored. The compounds were practically inactive towards DPPH radicals; Zn(II) complex **1** was the most active compound towards ABTS radicals, albeit moderately active when compared with the reference compound trolox. Concerning the activity towards H_2O_2, the compounds were found more active than the reference compound L-ascorbic acid, **H_2L** being by far the most active (H_2O_2% = 87.98 ± 0.46%) among the compounds.

In conclusion, the phenolic quinazoline derivative **H_2L** and its two complexes present differentiated biological properties when compared to their pyridine quinazoline analogues which bear the skeleton of (*E*)-4-(2-((pyridin-2-yl)methylene)hydrazinyl)quinazoline. Apart from the structural differences and the diversity of deprotonation states, the herein reported compounds presented negligible cleavage activity of plasmid DNA and lower antioxidant potency but much higher affinity for CT DNA, a fact that may include them to potential candidates targeting DNA.

Abbreviations

ABTS	2,2′-Azinobis-(3-ethylbenzothiazoline-6-sulfonic acid)
BHT	Butylated hydroxytoluene
BSA	Bovine serum albumin
CT	Calf-thymus
DPPH	1,1-Diphenyl-picrylhydrazyl
EB	Ethidium bromide
K	BSA-binding constant
K_b	DNA-binding constant
k_q	Quenching constant
K_{SV}	Stern–Volmer constant
MC	Metallacrown
Mcor	Metallacoronate
NDGA	Nordihydroguaiaretic acid
pDNA	pBR322 plasmid DNA
SA	Serum albumin.

Data availability

The data supporting this article have been included as part of the ESI.†

CCDC 2401516–2401518 contain the supplementary crystallographic data for the complexes.†

Conflicts of interest

There are no conflicts to declare.

References

1 P. Chellan and P. J. Sadler, *Philos. Trans. R. Soc., A*, 2015, **373**, 2014018.
2 G. Crisponi, V. M. Nurchi, D. Fanni, C. Gerosa, S. Nemolato and G. Faa, *Coord. Chem. Rev.*, 2010, **254**, 876–889.
3 M. Jarosz, M. Olbert, G. Wyszogrodzka, K. Młyniec and T. Librowski, *Inflammopharmacology*, 2017, **25**, 11–24.
4 C. P. Larson, U. R. Saha and H. Nazrul, *PLoS Med.*, 2009, **6**, e1000175.
5 W. X. Tian, S. Yu, M. Ibrahim, A. W. Almonaofy, L. He, Q. Hui, Z. Bo, B. Li and G. L. Xie, *J. Microbiol.*, 2012, **50**, 586–593.
6 S. Medici, M. Peana, V. M. Nurchi, J. I. Lachowicz, G. Crisponi and M. A. Zoroddu, *Coord. Chem. Rev.*, 2015, **284**, 329–350.
7 A. Rivero-Müller, A. De Vizcaya-Ruiz, N. Plant, L. Ruiz and M. Dobrota, *Chem.-Biol. Interact.*, 2007, **165**, 189–199.
8 J. d'Angelo, G. Morgant, N. E. Ghermani, D. Desmaële, B. Fraisse, F. Bonhomme, E. Dichi, M. Sghaier, Y. Li, Y. Journaux and J. R. J. Sorenson, *Polyhedron*, 2008, **27**, 537–546.
9 Q. Zhou, T. W. Hambley, B. J. Kennedy, P. A. Lay, P. Turner, B. Warwick, J. R. Biffin and H. L. Regtop, *Inorg. Chem.*, 2000, **39**, 3742–3748.
10 H. Abu Ali, S. N. Omar, M. D. Darawsheh and H. Fares, *J. Coord. Chem.*, 2016, **69**, 1110–1122.
11 C. I. Chukwuma, S. S. Mashele, K. C. Eze, G. R. Matowane, S. M. Islam, S. L. Bonnet, A. E. M. Noreljaleel and L. M. Ramorobi, *Pharmacol. Res.*, 2020, **155**, 104744.
12 M. Porchia, M. Pellei, F. Del Bello and C. Santini, *Molecules*, 2020, **25**, 5814.
13 B. Chudzik, I. B. Tracz, G. Czernel, M. J. Fiołka, G. Borsuk and M. Gagoś, *Eur. J. Pharm. Sci.*, 2013, **49**, 850–857.
14 J. Nagaj, R. Starosta and M. Jezowska-Bojczuk, *J. Inorg. Biochem.*, 2015, **142**, 68–74.
15 E. G. Geromichalou, D. T. Trafalis, P. Dalezis, G. Malis, G. Psomas and G. D. Geromichalos, *J. Inorg. Biochem.*, 2022, **231**, 111805.
16 O. A. Zalevskaya and Y. A. Gur'eva, *Russ. J. Coord. Chem.*, 2021, **47**, 861–880.
17 G. Psomas, A. J. Stemmler, C. Dendrinou-Samara, J. J. Bodwin, M. Schneider, M. Alexiou, J. W. Kampf, D. P. Kessissoglou and V. L. Pecoraro, *Inorg. Chem.*, 2001, **40**, 1562–1570.
18 A. Tarushi, C. P. Raptopoulou, V. Psycharis, C. K. Kontos, D. P. Kessissoglou, A. Scorilas, V. Tangoulis and G. Psomas, *Eur. J. Inorg. Chem.*, 2016, **2016**, 219–231.

19 A. Tarushi, A. G. Hatzidimitriou, M. Estrader, D. P. Kessissoglou, V. Tangoulis and G. Psomas, *Inorg. Chem.*, 2017, **56**, 7048–7057.
20 A. Tarushi, M. Zampakou, S. Perontsis, K. Lafazanis, A. A. Pantazaki, A. G. Hatzidimitriou, G. D. Geromichalos and G. Psomas, *Inorg. Chim. Acta*, 2018, **483**, 579–592.
21 A. Tarushi, G. D. Geromichalos, K. Lafazanis, C. P. Raptopoulou, V. Psycharis, N. Lalioti, A. A. Pantazaki, D. P. Kessissoglou, V. Tangoulis and G. Psomas, *New J. Chem.*, 2018, **42**, 6955–6967.
22 O. S. Vynohradov, V. A. Pavlenko, I. O. Fritsky, I. A. Gural'skiy and S. Shova, *Russ. J. Inorg. Chem.*, 2020, **65**, 1481–1488.
23 S. Lin, S. X. Liu, Z. Chen, B. Z. Lin and S. Gao, *Inorg. Chem.*, 2004, **43**, 2222–2224.
24 W. Yang, H. Yang, Q. Yao, S. Zeng, D. Li and J. Dou, *Inorg. Chem. Commun.*, 2017, **82**, 16–19.
25 H. Yang, Y. Q. Zhang, L. Sun, D. C. Li, S. Y. Zeng, Y. W. Li, Y. Yang and J. M. Dou, *Eur. J. Inorg. Chem.*, 2021, **2021**, 740–747.
26 H. Yang, Q. X. Yao, Y. W. Li, D. C. Li and J. M. Dou, *Dalton Trans.*, 2014, **43**, 16986–16991.
27 H. Yang, F. Cao, D. Li, S. Zeng, Y. Song and J. Dou, *Chem. – Eur. J.*, 2015, **21**, 14478–14485.
28 H. Yang, D. Li, S. Zeng and J. Dou, *Inorg. Chem. Commun.*, 2015, **58**, 84–86.
29 G. J. Chen, C. Y. Gao, W. Gu, X. Liu, S. P. Yan, J. L. Tian and D. Z. Liao, *Z. Anorg. Allg. Chem.*, 2011, **637**, 374–376.
30 S. Lin, S. X. Liu, J. Q. Huanga and C. C. Lina, *J. Chem. Soc., Dalton Trans.*, 2002, 1595–1601.
31 S. Da Su, X. M. Ou-Yang, K. K. Guo, Q. M. Lin, Y. Li, K. Wang, S. Y. Luo and F. P. Liang, *J. Cluster Sci.*, 2019, **30**, 863–868.
32 Y. Chen, J. Dou, D. Li and S. Wang, *Inorg. Chem. Commun.*, 2010, **13**, 167–170.
33 S. Lin, S. X. Liu and B. Z. Lin, *Inorg. Chim. Acta*, 2002, **328**, 69–73.
34 A. Majumder, S. Goswami, S. R. Batten, M. S. El Fallah, J. Ribas and S. Mitra, *Inorg. Chim. Acta*, 2006, **359**, 2375–2382.
35 G. C. Giri, S. Haldar, A. K. Ghosh, P. Chowdhury, L. Carrella, U. Ghosh and M. Bera, *J. Mol. Struct.*, 2017, **1142**, 175–184.
36 A. Beyer, M. S. von Gernler, S. Pflock, G. Türkoglu, L. Müller, A. Zahl, K. Gieb, P. Müller, T. Drewello and N. Burzlaff, *Eur. J. Inorg. Chem.*, 2018, **2018**, 765–777.
37 A. Tarushi, F. Kastanias, V. Psycharis, C. P. Raptopoulou, G. Psomas and D. P. Kessissoglou, *Inorg. Chem.*, 2012, **51**, 7460–7462.
38 E. Colacio, M. Ghazi, R. Kivekäs and J. M. Moreno, *Inorg. Chem.*, 2000, **39**, 2882–2890.
39 A. Lakma, R. N. Pradhan, S. M. Hossain, J. van Leusen, P. Kögerler and A. K. Singh, *Inorg. Chim. Acta*, 2019, **486**, 88–94.
40 C. Kakoulidou, A. G. Hatzidimitriou, K. C. Fylaktakidou and G. Psomas, *Polyhedron*, 2021, **195**, 114986.
41 C. Kakoulidou, C. T. Chasapis, A. G. Hatzidimitriou, K. C. Fylaktakidou and G. Psomas, *Dalton Trans.*, 2022, **51**, 16688–16705.
42 C. Kakoulidou, V. R. Kosmas, A. G. Hatzidimitriou, K. C. Fylaktakidou and G. Psomas, *J. Inorg. Biochem.*, 2021, **219**, 111448.
43 C. Kakoulidou, P. S. Gritzapis, A. G. Hatzidimitriou, K. C. Fylaktakidou and G. Psomas, *J. Inorg. Biochem.*, 2020, **211**, 111194.
44 A. Jori, S. R. Dixit and G. V. Pujar, *Asian – J. Chem.*, 2020, **32**, 2617–2623.
45 S. I. Kovalenko, L. M. Antypenko, A. K. Bilyi, S. V. Kholodnyak, O. V. Karpenko, O. M. Antypenko, N. S. Mykhaylova, T. I. Los and O. S. Kolomoyets, *Sci. Pharm.*, 2012, **81**, 359–392.
46 T. V. Trashakhova, E. V. Nosova, P. A. Slepukhin, M. S. Valova, G. N. Lipunova and V. N. Charushin, *Russ. Chem. Bull.*, 2011, **60**, 2302–2307.
47 H. Yamada, A. Shirai, K. Kato, J. Kimura, H. Ichiba, T. Yajima and T. Fukushima, *Chem. Pharm. Bull.*, 2010, **56**, 875–878.
48 J. Marmur, *J. Mol. Biol.*, 1961, **3**, 208–218.
49 M. E. Reichmann, S. A. Rice, C. A. Thomas and P. Doty, *J. Am. Chem. Soc.*, 1954, **76**, 3047–3053.
50 *Apex2 Version 2 User Manual M86-E01078*, Bruker Analytical X-ray Systems Inc., 2006, preprint.
51 *SADABS: Area–Detector Absorption Correction*, Siemens Industrial Automation Inc.
52 L. Palatinus and G. Chapuis, *J. Appl. Crystallogr.*, 2007, **40**, 786–790.
53 P. W. Betteridge, J. R. Carruthers, R. I. Cooper, K. Prout and D. J. Watkin, *J. Appl. Crystallogr.*, 2003, **36**, 1487–1487.
54 W. J. Geary, *Coord. Chem. Rev.*, 1971, **7**, 81–122.
55 K. Nakamoto, *Infrared and Raman Spectra of Inorganic and Coordination Compounds: Part B: Applications in Coordination, Organometallic, and Bioinorganic Chemistry*, 2008, 1–408.
56 B. J. Hathaway, in *Comprehensive Coordination Chemistry*, ed. G. Wilkinson, Pergamon Press, Oxford, UK, 1987, vol. 5, pp. 533–773.
57 A. W. Addison, T. N. Rao, J. Reedijk, J. Van Rijn and G. C. Verschoor, *J. Chem. Soc., Dalton Trans.*, 1984, 1349–1356.
58 A. Wolfe, G. H. Shimer and T. Meehan, *Biochemistry*, 1987, **26**, 6392–6396.
59 A. Dimitrakopoulou, C. Dendrinou-Samara, A. A. Pantazaki, M. Alexiou, E. Nordlander and D. P. Kessissoglou, *J. Inorg. Biochem.*, 2008, **102**, 618–628.
60 A. M. Pizarro and P. J. Sadler, *Biochimie*, 2009, **91**, 1198–1211.
61 J. L. Garcia-Gimenez, M. Gonzalez-Alvarez, M. Liu-Gonzalez, B. Macías, J. Borras and G. Alzuet, *J. Inorg. Biochem.*, 2009, **103**, 923–934.
62 J. R. Lakowicz, *Principles of fluorescence spectroscopy*, Springer, 2006.
63 D. P. Heller and C. L. Greenstock, *Biophys. Chem.*, 1994, **50**, 305–312.

64 C. Kontogiorgis, M. Ntella, L. Mpompou, F. Karallaki, P. Athanasios, D. Hadjipavlou-Litina and D. Lazari, *J. Enzyme Inhib. Med. Chem.*, 2016, **31**, 154–159.
65 M. M. Gineinah, M. A. El-Sherbeny, M. N. Nasr and A. R. Maarouf, *Arch. Pharm.*, 2002, **335**, 556–562.
66 A. M. Alafeefy, A. A. Kadi, O. A. Al-Deeb, K. E. H. El-Tahir and N. A. Al-Jaber, *Eur. J. Med. Chem.*, 2010, **45**, 4947–4952.
67 S. Dairi, M. A. Carbonneau, T. Galeano-Diaz, H. Remini, F. Dahmoune, O. Aoun, A. Belbahi, C. Lauret, J. P. Cristol and K. Madani, *Food Chem.*, 2017, **237**, 297–304.
68 B. M. Ali, M. Boothapandi and A. S. Sultan Nasar, *Data Brief*, 2020, **28**, 104972.
69 M. Wettasinghe and F. Shahidi, *Food Chem.*, 2000, **70**, 17–26.
70 R. E. Olson and D. D. Christ, *Annu. Rep. Med. Chem.*, 1996, **31**, 327–336.
71 L. Stella, A. L. Capodilupo and M. Bietti, *Chem. Commun.*, 2008, 4744–4746.
72 O. H. Laitinen, V. P. Hytönen, H. R. Nordlund and M. S. Kulomaa, *Cell. Mol. Life Sci.*, 2006, **63**, 2992–3017.
73 G. Sudlow, D. J. Birkett and D. N. Wade, *Mol. Pharmacol.*, 1976, **12**, 1052–1061.
74 M. Lazou, A. Tarushi, P. Gritzapis and G. Psomas, *J. Inorg. Biochem.*, 2020, **206**, 111019.